nature nanotechnology

LETTERS

PUBLISHED ONLINE: 7 JUNE 2009 | DOI: 10.1038/NNANO.2009.122

Observation of the triplet exciton in EuS-coated single-walled nanotubes

Aditya D. Mohite[1], Tiffany S. Santos[2†], Jagadeesh S. Moodera[2] and Bruce W. Alphenaar[1*]

Photon absorption by carbon nanotubes creates bound electron–hole pairs called excitons[1–8], which can exist in spin-polarized triplet or spin-unpolarized singlet configurations. Triplet excitons are optically inactive owing to the weak spin–orbit coupling in nanotubes. This prevents the optical injection of electron spin into nanotubes for spintronic applications[9] and limits the efficiency of photocurrent generation[10]. Here, we show that it is possible to optically excite the triplet exciton by using a ferromagnetic semiconductor as a spin filter[11] to mix the singlet and triplet excitons. The triplet contribution to the photocurrent is detected, representing the first direct evidence of the triplet exciton in carbon nanotubes.

In the photoexcitation process, an absorbed photon promotes an electron into a higher energy state, and the excited electron leaves behind a positively charged hole. If the photon energy corresponds to the energy spacing between one-dimensional sub-bands, there is a small probability that the photon absorption process will produce a freely mobile electron–hole pair (an interband transition)[2]. However, owing to strong Coulomb interactions, the dominant absorption mechanism in carbon nanotubes is the formation of bound electron–hole pairs known as excitons[1,2,6–8]. The photon energy required for exciton formation lies below the interband transition energy by an amount equal to the exciton binding energy. There are a series of excitons for each possible interband transition, but under normal experimental conditions, momentum/spin conservation and parity considerations allow for only one of these to be optically active.

Figure 1a shows the lowest energy interband transition (S_{11}) for a chiral nanotube, together with the transition energies for the three lowest energy excitons ($^1E_{11}$, $^1D_{11}$ and $^3E_{11}$). The subscript indices give the sub-bands over which the transition occurs (in this case, between the highest energy occupied sub-band and the lowest energy unoccupied sub-band). The total spin of the exciton is determined by the electron and hole spin states, which can be combined in four different possible ways. One of these combinations has zero spin, and is known as the singlet exciton; three have finite spin, and together form the triplet exciton[12]. In Fig. 1a, the superscript (1 or 3) indicates whether the exciton spin state is a singlet or a triplet. All the triplet excitons (including $^3E_{11}$ in Fig. 1a) are usually optically inactive, because photons themselves have zero spin. Of the singlet excitons only $^1E_{11}$ is optically active because $^1D_{11}$ (the so-called dark exciton, where D stands for dark) has the wrong parity for photon absorption. The $^1D_{11}$ exciton can be made optically active, however, under high magnetic field[5,13]. Here we demonstrate the optical excitation and electrical detection of the $^3E_{11}$ exciton.

The device structure used in our experiments is shown in Fig. 1b. Carbon nanotubes grown by chemical vapour deposition (1.3–2.1 nm in diameter) were randomly distributed on an oxidized silicon substrate, with a coverage of ~1 nanotube per 100 μm^2. The nanotubes were then coated with a 3-nm-thick layer of EuS, followed by a 3-nm-thick ytrrium protective layer and a 6-nm-thick aluminium contact. Optical characterization was performed using a recently developed capacitive photocurrent technique[14–18]. The sample was fixed to a copper block within an optical flow cryostat, which was placed between the poles of an electromagnet. Tunable pulsed laser light was directed through the thin aluminium/yttrium/EuS contact layer and onto the carbon nanotubes. A photon absorbed in the nanotube creates one of the electron–hole pair states shown in Fig. 1a (higher sub-band

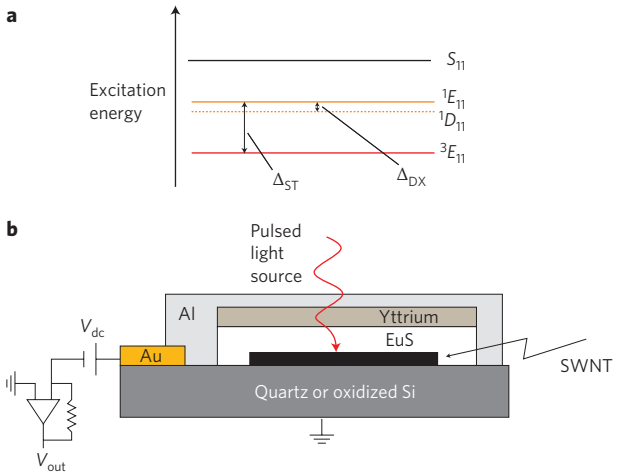

Figure 1 | Carbon nanotube optical transition energies and measurement geometry. a, Excitation energy diagram for the experimentally measured transitions. The solid black line shows the lowest lying interband transition (S_{11}). The three lowest energy excitons ($^1E_{11}$, $^1D_{11}$, $^3E_{11}$) associated with the S_{11} transition are indicated by orange lines for the singlet excitons ($^1E_{11}$ and $^1D_{11}$), and a red line for the triplet exciton ($^3E_{11}$). Solid lines show excitons ($^1E_{11}$ and $^3E_{11}$) corresponding to the bonding-like combination of the K-point and K′-point states, and the dashed line shows the so-called dark exciton ($^1D_{11}$), corresponding to the anti-bonding-like combination of the K-point and K′-point states. (The K and K′ points are the two conduction band valleys of graphene, each of which is composed from three equivalent corners of the graphene Brillouin zone.) Also shown are the light–dark (Δ_{DX}) and singlet–triplet (Δ_{ST}) zero-field energy splitting. **b**, Schematic of the device configuration used in the capacitive photocurrent measurements. The single-walled nanotube (SWNT) is grown on an oxidized silicon or quartz substrate and coated with a EuS/yttrium tunnel barrier, followed by an aluminium contact. Pulsed laser light is directed at the nanotube, and the resulting a.c. signal V_{out} is amplified and measured. A d.c. bias V_{dc} is applied to encourage exciton dissociation.

[1]Department of Electrical and Computer Engineering, University of Louisville, Louisville, Kentucky 40292, USA, [2]Francis Bitter Magnet Laboratory, Massachusetts Institute of Technology, Cambridge, Massachusetts 02139, USA; †Present address: Center for Nanoscale Materials, Argonne National Laboratory, Argonne, Illinois 60439, USA. *e-mail: brucea@louisville.edu

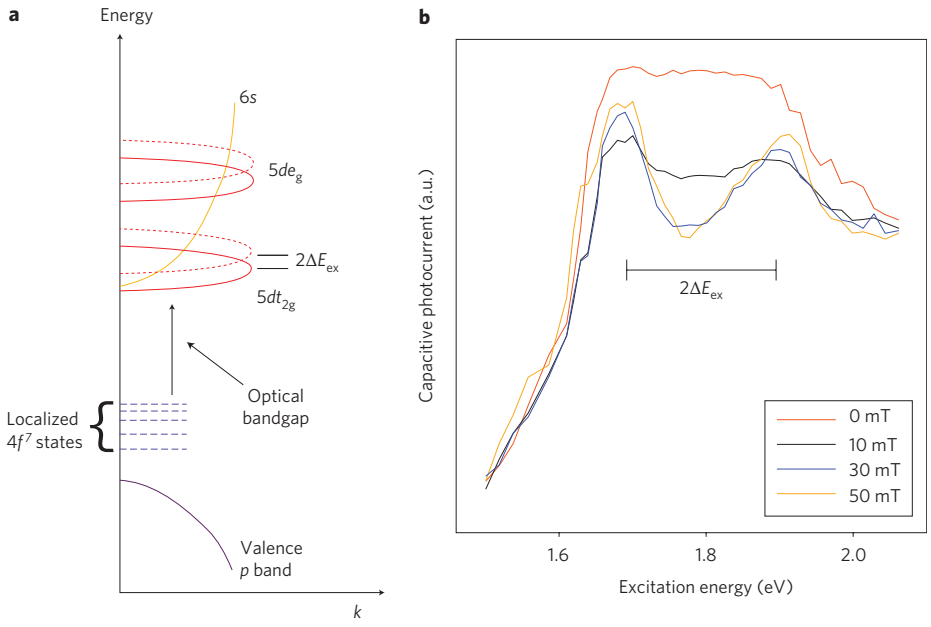

Figure 2 | Europium sulphide (EuS) energy diagram and capacitive photocurrent spectrum. a, Energy diagram of EuS showing energy as a function of momentum, *k*. Blue, red and yellow lines represent states with principle quantum numbers 4, 5 and 6, respectively, and the valence band is shown in purple. Spin polarization of the localized $4f^7$ states results in an exchange splitting $2\Delta E_{ex}$ of the $5dt_{2g}$ states forming the conduction band. The optical bandgap is determined by the energy separation between the $4f^7$ states and the $5dt_{2g}$ states. Although not involved in the optical transition, the 6s and $5de_g$ states are shown for completeness. **b**, Capacitive photocurrent spectrum of the EuS film for four different applied fields. The field is applied parallel to the EuS film. The exchange splitting $2\Delta E_{ex}$ becomes visible as the magnetic field increases to 10 mT. Above 30 mT, the EuS magnetization is complete, and the spectrum no longer changes with increasing magnetic field.

transitions are too energetic to be considered). Upon decay, one of the charges may tunnel into the aluminium contact, causing an additional potential to be measured. Similarly, electron–hole pairs may also be generated in the EuS (Fig. 2a) and contribute a contact potential. By keeping the laser spot size smaller than the nanotube separation distance, individual nanostructures can be probed.

Capacitive photocurrent measurements were first made on a EuS film with no carbon nanotube present. EuS is one of the europium chalcogenides, a wide-bandgap semiconductor that undergoes a ferromagnetic transition at cryogenic temperatures[11,19]. The energy diagram for EuS is shown in Fig. 2a. The gap between the $4f^7$ states and the $5dt_{2g}$ states defines the optical bandgap. Below a temperature of 16.6 K, the half-filled $4f^7$ states become ferromagnetically ordered. Exchange interaction in turn causes the conduction band to split into two energy levels, separated by the exchange energy $2\Delta E_{ex}$. Figure 2b shows the capacitive photocurrent spectrum of a EuS film on an oxidized silicon substrate, cooled in zero magnetic field to a temperature of 8 K. The capacitive photocurrent increases sharply at an excitation energy of ~1.5 eV, which marks the optical bandgap[20]. When the magnetic field is increased to 30 mT, two peaks are formed, corresponding to the up and down spin levels of the $5dt_{2g}$ states.

These experiments show that the EuS spins are polarized under application of a 30 mT magnetic field. Next, we repeat the polarization in the presence of a carbon nanotube (Fig. 3). The sample is first cooled to 8 K at zero magnetic field to randomly orient the spins of the EuS. In this configuration, the nanotube spectrum is indistinguishable from that measured without the EuS being present[14]. Two peaks are observed (bottom panel of Fig. 3a), corresponding to the $^1E_{11}$ exciton and the interband S_{11} transition, respectively. As described in ref. 14 (see also Supplementary Fig. S1), the ground-state excitonic capacitive photocurrent peak has a Fowler–Nordheim type bias dependence, corresponding to field-assisted tunnelling through the potential created by the exciton binding energy. The measurements in Fig. 3 were performed with 10 V d.c. bias across the substrate to encourage exciton dissociation. The energy difference between the excitonic and interband peaks provides a measure of the exciton binding energy. Recent experiments have shown that the binding energy is approximately given by x/d, where d is the nanotube diameter in nanometres, and x is proportional to the inverse dielectric constant of the environment[21,22]. For nanotubes in free space x is found to be 450 meV (ref. 22), whereas for nanotubes in a PMOAVE polymer matrix, $x = 340$ meV (ref. 21). Our results give an average value for x of 243 meV, which is reasonable considering the increase in dielectric constant of the SiO_2 ($\varepsilon_r = 3.9$) compared with PMOAVE ($\varepsilon_r = 2.5$)[2].

The application of a small magnetic field to align the spins in the EuS film results in the appearance of a new, low-energy peak. The new peak grows with increasing magnetic field, until spin alignment in the EuS is complete at 30 mT. The field also causes the interband S_{11} peak to redshift by ~6 meV. This shift is most likely due to the magnetization of the EuS contact, which produces an Aharonov–Bohm (AB) flux along the nanotube axis[23]. Assuming a standard value for the AB shift of 1 meV per Tesla[24], this implies that the EuS generates a field of ~6 T, and gives a relative permeability for EuS of ~200, in agreement with previously measured values[25]. Figure 3b is an image plot detailing the emergence of the new peak with increasing field. As shown in Supplementary Table S1, similar results were observed in measurements of four different nanotubes taken from four different growth runs.

The emergence of the low-energy peak indicates that the alignment of the spins in the EuS causes either the dark exciton $^1D_{11}$ or the triplet exciton $^3E_{11}$ lying below $^1E_{11}$ to become optically active. It can be shown, however, that the dark exciton does not have the correct energy or magnetic field dependence to explain

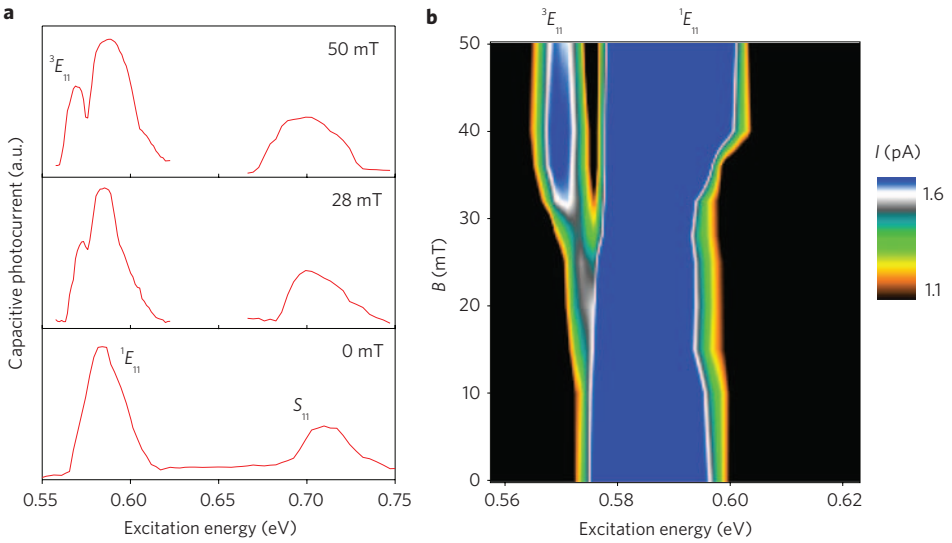

Figure 3 | Capacitive photocurrent spectrum of EuS-coated single-walled nanotube. a, Capacitive photocurrent spectra of a EuS-coated single-walled nanotube for three different applied magnetic fields. The field is applied parallel to the EuS film, and no effort was made to align the field direction with the nanotube axis. At zero field, peaks are observed corresponding to the light singlet ($^1E_{11}$) and interband (S_{11}) transitions. As the field increases, the EuS is magnetized, causing a new peak to appear, corresponding to the $^3E_{11}$ triplet transition. The field also causes the S_{11} transition to shift, presumably due to the Aharanov–Bohm flux through the tube. To decrease the rather lengthy measurement time, the energy region between the $^1E_{11}$ and S_{11} peaks was not measured in all runs (see top two panels). Earlier experiments demonstrate that this region is unchanged by the magnetic field. **b**, Image plot showing the emergence of the triplet exciton peak with increasing magnetic field. The plot was formed from a series of spectra of capacitive photocurrent, *I*, obtained at different magnetic fields, *B*. The measured singlet–triplet energy splitting is 24 meV.

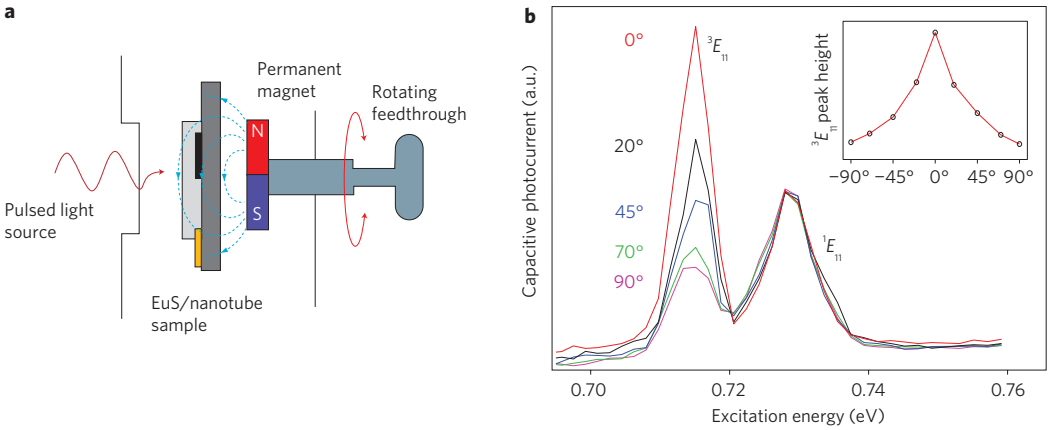

Figure 4 | Magnetic field orientation dependence of the triplet peak height. a, Measurement configuration used to rotate the polarization of the spin orientation in the EuS film. A permanent niodymium ring magnet is placed behind the sample and rotated with respect to the nanotube axis. **b**, Capacitive photocurrent as a function of magnetic orientation. The $^3E_{11}$ triplet peak grows as the field is oriented parallel to the nanotube axis. The $^1E_{11}$ singlet peak and the singlet–triplet energy spacing remain unchanged. The inset shows the $^3E_{11}$ peak height as a function of magnetic field orientation.

the new peak. Others have demonstrated[13] that the dark-light energy splitting Δ_{ld} is given by

$$\Delta_{ld}^2 = \Delta_{DX}^2 + (\mu\pi d^2 B_{\|}/4)^2 \quad (1)$$

Here, Δ_{DX} (Fig. 1a) is the zero field splitting, μ is a coupling constant (ranging from 0.4–1.0 meV T^{-1} nm^{-2}), d is the nanotube diameter and $B_{\|}$ is the magnetic field pointing parallel to the nanotube axis. The zero field splitting Δ_{DX} has a $1/d$ dependence, decreasing from 4 to 1 meV as the tube diameter increases from 1 to 1.3 nm. This suggests that in our larger diameter (1.3 to 2.1 nm) nanotubes, Δ_{DX} should be less than 1 meV. The measured energy splitting, however, is more than an order of magnitude larger than this, ranging from 14 to 23 meV (see Supplementary Fig. S2). To achieve this would require a magnetic field of between 100 and 300 T, much larger than the field produced by the EuS (ref. 26).

Some of this difference could be due to the dielectric medium in which the nanotube is located[27]. (Our samples are grown on oxidized silicon, whereas those of ref. 10 are micelle encapsulated tubes on quartz.) However, the $^1E_{11}$ values we observe (0.73–0.57 eV for 1.3–2.1 nm diameter tubes) follow the same $1/d$ dependence as those observed in ref. 13 (1.1–0.8 eV for 1.0–1.3 nm diameter nanotubes), suggesting that the dielectric constants are not substantially different in the two experiments. The observed order of magnitude increase in Δ_{DX} is difficult to account for in this way.

In addition to the wrong energy spacing, the dark exciton also has the wrong magnetic field dependence to explain the new peak. As seen in equation (1), the light–dark splitting is strongly dependent on the orientation of the magnetic field with respect to the nanotube axis. To test for this effect in the EuS-coated nanotubes, we used the measurement setup shown in Fig. 4a. A permanent neodymium ring magnet was placed behind the sample. The magnetic orientation of the EuS contact could then be rotated with respect to the carbon nanotube axis by rotating the orientation of the fixed magnet. The results are shown in Fig. 4b. The magnitude of the low-energy peak increases by a factor of three as the magnetic field is rotated to lie parallel to the nanotube axis. The maximum peak height thus occurs as the EuS magnetization aligns with the natural spin orientation of the carbon nanotube. However, the splitting between the two peaks, as well as the magnitude of the $^1E_{11}$ peak, remain constant. This is not what would be expected for the magnetic field orientation dependence of the light–dark splitting (as observed in ref. 13). We must therefore conclude that the new peak is instead due to the $^3E_{11}$ triplet exciton.

In a variety of systems, mixing between the singlet and triplet states has been induced by the large orbital angular momentum of a heavy metal compound[28–30]. For example, iridium compounds are used to induce singlet–triplet decay in conjugated polymers[31]. It is possible then that the close proximity of the heavy Eu atoms to the nanotube induces singlet–triplet mixing among the nanotube excitons. This hypothesis implies that the EuS is merely a source for spin–orbit coupling, which could also be provided by any number of heavy metal compounds. In fact, heavy metals (that is, gold, titanium, platinum and palladium) are typically used to make contact to carbon nanotubes. Despite this, no previous evidence for the triplet peak has been observed[32]. An alternative mechanism for triplet enhancement is exchange interaction between the nanotube and EuS states. This mechanism has been shown to apply for an aromatic molecule (M) in the presence of a paramagnetic molecule (such as O_2 or NO_2)[33–35]. In our case, the nanotube singlet ($^1E_{11}$) and triplet ($^3E_{11}$) states can couple with the localized spin polarized ground state occupied by the $4f^7$ electrons of the Eu^{2+} magnetic ions in the EuS (ref. 26). Once again, there will be strong exchange interactions mixing the coupled states, depending on the orientation of the electron spins in the EuS/nanotube complex. This coupling will allow the $^3E_{11}$ exciton to take on some of the singlet character of the $^1E_{11}$, causing enhancement in the absorbance. Calculations are required to confirm the existence of this effect in the EuS-coated nanotubes.

The method presented here can be applied to other excitonic systems that are limited by the ability to optically excite and detect the triplet exciton, such as organic photovoltaic materials. In this way, improvement of the photocurrent efficiency due to additional absorption into the triplet exciton could be achieved[10]. In addition, the method provides a mechanism for the optical injection of spin-polarized electron–hole pairs in carbon nanotubes and other nanoscale structures. Optical spin injection has been highly successful for III/V semiconductors[36], but carbon nanotube spin electronics has been forced to rely on low-yield ferromagnetic contacting schemes[9]. The EuS contact can also be used as a means to filter spin-polarized electrons for spin injection and detection.

Methods

Nanotubes were grown on either quartz or oxidized silicon substrates using the chemical vapour deposition method. A solution of iron (III) nitrate in isopropyl alcohol was dispersed on the substrate by dipping the sample in the catalyst solution followed by a hexane rinse. The samples were then heated in a tube furnace to 890 °C. Reduction of the catalyst particles was carried out by flowing hydrogen argon gas at 100 s.c.c.m., after which the nanotubes were grown using methane gas at 100 s.c.c.m. for 5–7 minutes. Nanotube distribution and diameter was determined using a combination of atomic force microscopy and Raman spectroscopy. In analysing the Raman spectra, the relation $\rangle_{RBM} = A/d + B$ was used, where $A = 234\ cm^{-1}$, $B = 10\ cm^{-1}$, $\rangle_{RBM}$ is the radial breathing mode and d is the nanotube diameter.

EuS films were prepared in a high vacuum deposition chamber with a base pressure of 6×10^{-8} torr. The EuS layer was deposited at room temperature by electron-beam evaporation from a EuS pellet. The over layers of yttrium, aluminium and gold were subsequently deposited. Appropriate shadow metal masks were used to create the EuS film and the gold electrodes away from the quartz/oxidized silicon substrate edges, with the partial overlap of the gold with the aluminium/yttrium/EuS as shown in Fig. 1b. A thin layer of Al_2O_3 deposited over the whole area was used to protect the structure. The entire sample was prepared *in situ*.

Optical characterization was carried out using a Spectra-Physics optical parametric amplifier (OPA) pumped by a 130 fs pulsed Ti:sapphire laser with a repetition rate of 1 kHz. The excitation energy was tunable from 0.4 to 4 eV. It was therefore possible to observe both the EuS and nanotube spectra at a single laser position. The nanotubes were located by first setting the excitation energy to the $^1E_{11}$ exciton (~0.6 eV for a 1.6-nm-diameter nanotube), and then searching for a response in the capacitive photocurrent while scanning the laser spot over the sample surface. During the measurement, a bias of 10 V was applied between the contact and substrate ground to encourage exciton dissociation. Once a signal was detected, the laser polarization was rotated to maximize the signal and to ensure that only a single nanotube was being measured (see ref. 14). If more than one nanotube was present, additional capacitive photocurrent peaks would appear as the polarization aligned with the various nanotube axes. The signal strength is proportional to the excited charge density multiplied by the charge separation distance. The wavelength resolution and sensitivity obtained is similar to a standard photo-absorption measurement.

The peak assignment was made by comparing the bias dependence of the two peaks. The excitonic peak height ($^1E_{11}$) increases sharply with increasing bias, whereas the interband transition (S_{11}) shows no bias dependence. Note that the S_{11} and $^1E_{11}$ peak heights are comparable in magnitude. This is in contrast to nanotube absorption or luminescence measurements where the exciton is completely dominant over the interband transition. In the capacitive photocurrent measurement, the ease with which free carriers are collected by the contact compensates for the relatively low oscillator strength of the interband transition.

Received 23 January 2009; accepted 28 April 2009; published online 7 June 2009

References

1. Ando, T. Excitons in carbon nanotubes. *J. Phys. Soc. Jpn* **66,** 1066–1073 (1997).
2. Wang, F., Dukovic, G., Brus, L. E. & Heinz, T. F. Optical resonances in carbon nanotubes arise from excitons. *Science* **308,** 838–841 (2005).
3. Maultzsch, J. *et al.* Exciton binding energies in carbon nanotubes from two-photon photoluminescence. *Appl. Phys. Lett.* **72,** 241402 (2005).
4. Zhao, H. & Mazumdar, S. Electron–electron interaction effects on the optical excitations of semiconducting single-walled carbon nanotubes. *Phys. Rev. Lett.* **93,** 157402 (2004).
5. Ando, T. Effects of valley mixing and exchange on excitons in carbon nanotubes with Aharonov–Bohm flux. *J. Phys. Soc. Jpn* **75,** 024707 (2006).
6. Spataru, C. D., Ismail-Beigi, S., Benedict, L. X. & Louie, S. G. Excitonic effects and optical spectra of single-walled carbon nanotubes. *Phys. Rev. Lett.* **92,** 077402 (2004).
7. Perebeinos, V., Tersoff, J. & Avouris, P. Radiative lifetime of excitons in carbon nanotubes. *Nano Lett.* **5,** 2495–2499 (2005).
8. Barros, E. B. *et al.* Selection rules for one- and two-photon absorption by excitons in carbon nanotubes. *Phys. Rev. B* **73,** 241406(R) (2006).
9. Tsukagoshi, K., Alphenaar, B. W. & Ago, H. Coherent transport of electron spin in ferromagnetically contacted carbon nanotube. *Nature* **401,** 572–574 (1999).
10. Hu, X. & Hu, B. Photovoltaic processes of singlet and triplet excited states in organic solar cells. *Adv. Funct. Mater.* **18,** 2611–2617 (2008).
11. Moodera, J. S., Santos, T. S. & Nagahama, T. The phenomena of spin-filter tunneling. *J. Phys. Condens. Matt.* **18,** 1–24 (2006).
12. Tretiak, S. Triplet state absorption in carbon nanotubes: A TD–DFT study. *Nano Lett.* **7,** 2201–2206 (2007).
13. Srivastava, A., Htoon, H., Klimov, V. I. & Kono, J. Direct observation of dark excitons in individual carbon nanotubes: Inhomogeneity in the exchange splitting. *Phys. Rev. Lett.* **101,** 087402 (2008).
14. Mohite, A. D., Gopinath, P., Shah, H. M. & Alphenaar, B. W. Exciton dissociation and Stark effect in the carbon nanotube photocurrent spectrum. *Nano Lett.* **8,** 142–146 (2008).
15. Mohite, A., Lin, J.-T., Sumanasekera, G. & Alphenaar, B. W. Field enhanced photocurrent spectroscopy of excitonic states in single-wall carbon nanotubes. *Nano Lett.* **6,** 1369–1373 (2006).
16. Mohite, A. D. *et al.* Photocurrent spectroscopy of double-wall carbon nanotubes. *Chem. Phys. Lett.* **412,** 190–194 (2005).
17. Mohite, A., Gopinath, P., Chakraborty, S. & Alphenaar, B. W. Displacement current detection of photoconduction in carbon nanotubes. *Appl. Phys. Lett.* **86,** 061114 (2005).

18. Vaddiraju, S. *et al.* Mechanism of 1D crystal growth in reactive vapor transport: indium nitride nanowires. *Nano Lett.* **5,** 1625–1631 (2005).
19. Mauger, A. & Godart, C. The magnetic, optical and transport properties of representatives of a class of magnetic semiconductors: the europium chalcogenides. *Phys. Rep.* **141,** 51–176 (1986).
20. Dimmock, J. O. Optical properties of the europium chalcogenides. *IBM J. Res. Develop.* **14,** 301–308 (1970).
21. Dukovic, G. *et al.* Structural dependence of excitonic optical transitions and band-gap energies in carbon nanotubes. *Nano Lett.* **5,** 2314–2318 (2005).
22. Lefebvre, J. & Finnie, P. Polarized photoluminescence excitation spectroscopy of single-walled carbon nanotubes. *Phys. Rev. Lett.* **98,** 167406 (2007).
23. Ajiki, H. & Ando, T. Electronic states of carbon nanotubes. *J. Phys. Soc. Jpn* **62,** 1255–1266 (1993).
24. Zaric, S. *et al.* Excitons in carbon nanotubes with broken time-reversal symmetry. *Phys. Rev. Lett.* **96,** 016406 (2006).
25. McGuire, T. R. Magnetic properties of some divalent europium compounds. *J. Appl. Phys.* **34,** 1345–1346 (1963).
26. Hao, X., Moodera, J. S. & Meservey, R. A thin film superconductor in an exchange field. *Phys. Rev. Lett.* **67,** 1342–1345 (1991).
27. Ohno, Y. *et al.* Excitonic transition energies in single walled carbon nanotubes: dependence on environmental dielectric constant. *Phys. Stat. Sol. B* **244,** 4002–4005 (2007).
28. Kavarnos, G., Cole, T., Scribe, P., Dalton, J. & Turro, N. External heavy-atom induced spin–orbital coupling. Spectroscopic study of naphthonorbornanes. *J. Am. Chem. Soc.* **93,** 1032–1034 (1971).
29. Romanova, Z., Deshayes, K. & Piotrowiak, P. Remote intermolecular 'heavy-atom effect': spin–orbit coupling across the wall of a hemicarcerand. *J. Am. Chem. Soc.* **123,** 2444–2445 (2001).
30. Hu, B., Wu, Y., Zhang, Z., Dai, S. & Shen, J. Effects of ferromagnetic nanowires on singlet and triplet exciton fractions in fluorescent and phosphorescent organic semiconductors. *Appl. Phys. Lett.* **88,** 022114 (2006).
31. Shao, Y. & Yang, Y. Efficient organic heterojunction photovoltaic cells based on triplet materials. *Adv. Mater.* **17,** 2841–2844 (2005).
32. Freitag, M., Martin, Y., Misewich, J. A., Martel, R. & Avouris, P. H. Photoconductivity of single carbon nanotubes. *Nano Lett.* **3,** 1067–1071 (2003).
33. Hoijtink, G. J. The influence of paramagnetic molecules on singlet–triplet transitions. *Mol. Phys.* **3,** 67–70 (1960).
34. Murrell, J. N. The effect of paramagnetic molecules on the intensity of spin-forbidden absorption bands of aromatic molecules. *Mol. Phys.* **3,** 319–329 (1960).
35. Evans, D. F. Magnetic perturbation of singlet–triplet transitions. *J. Chem. Soc.* 3885–3888 (1957).
36. Pierce, D. T. *et al.* GaAs spin polarized electron source. *Rev. Sci. Instrum.* **51,** 478–499 (1980).

Acknowledgements

The authors thank S. Tretiak for theoretical guidance, and for his critical reading of this manuscript. Financial support was provided by the Office of Naval Research ONR N00014-06-1-0228 and ONR N00014-06-1-0235, the National Science Foundation NSF DMR 0504158 and the U.S. Department of Energy DE-FG02-07ER46375.

Author contributions

B.W.A. conceived the experiment and wrote the manuscript. A.D.M. performed the device fabrication and optical characterization. T.S.S. and J.S.M. performed material deposition. B.W.A., A.D.M. and J.S.M. designed the experiment, discussed the results and commented on the manuscript.

Additional information

Supplementary information accompanies this paper at www.nature.com/naturenanotechnology. Reprints and permission information is available online at http://npg.nature.com/reprintsandpermissions/. Correspondence and requests for materials should be addressed to B.W.A.